Supplementary materials

Main article available at https://doi.org/10.5802/crgeos.53

Materials and methods

We follow Spada and Galassi [2017], who examined global sea levels from 30,000 BP to today and key intermediate dates. We employ a Glacial Isostatic Adjustment (GIA) model to account for the Earth's deformation and gravity variations in response to glacial melting and for a "gravitationally self-consistent" reconstruction of the paleotopography [Peltier, 1994], using an iterative approach. In particular, the model extends the sea-level equation solver SELEN [Martinec et al., 2018, Spada and Melini, 2019] to any given coastline, taking into account the horizontal migration of shorelines, the transition between floating and grounded ice, and the rotational feedback on sea level. The computations adopt the latest version of the ice sheets chronology progressively developed by Kurt Lambeck and collaborators at the Australian National University [Lambeck and Chappell, 2001, Lambeck et al., 2002, 2003]. The Earth is spherically layered, with a viscosity increase by a factor of 10 between the upper and lower mantle. In our GIA runs, a uniform equal-area grid [Tegmark, 1996] with horizontal spatial resolution of 20 km is employed; the total integration interval is 30,000 years, with time increments of 500 years.

Data input models and variables include: (a) present day topography constrained by the National Oceanic and Atmospheric Administration's ETOPO1 global elevation database at 1 arc–minute resolution, (b) depth-dependence of density and rheological parameters (i.e., a spherically symmetric Earth model), (c) a set of "Love numbers" (measures of spherical viscoelasticity for the Earth originally conceived by Augustus Edward Hough Love) to a given maximum harmonic degree (e.g., $l_{\max} = 256$), (d) a model for the present day topography (ETOPO1) to define the present day ocean function, (e) a raster surface of the Earth on which the sea-level equation is discretized (global equal-area icosahedron-based spherical grid), and (f) information about the geometry of the ice sheets and about their time-evolution in the time window of interest (an "ice model"). Preliminary analyses employed ETOPO1 global elevation data [Amante and Eakins, 2009] mapped by Dobson [2014], including cartography by Jerry Whistler, University of Kansas, and a visualization developed by Zong [2015].

Other global GIA models exist, e.g. ICE-6G_C (VM5a) of Peltier et al. [2015]. With respect to the model adopted in this study, ICE-6G_C (VM5a) is characterised by different assumptions about the volume of the major ice sheets at the LGM, the chronology of de-glaciation, and the viscosity contrast between the upper and the lower mantle. Using SELEN, we have verified that, as long as we are concerned with the evolution of topography since the LGM, the two models provide consistent scenarios for the geometry of Beringia. This has been verified even across the Bering Strait, relatively close to the former Laurentide ice sheet, where ice distribution and volumes differ significantly in the two GIA models.

Uncertainty and sensitivity

How certain can we be that the Bering Transitory Archipelago actually existed? As real as they may seem on our maps and visualizations, these islands are generated by a model, not detected by the human eye or sensors of any sort. Our simulations are sensitive to spatial and temporal resolutions as well as ice history and other input data. A global run of ICE-5G (VM2) at LGM did not find the Bering Transitory Archipelago [Spada and Galassi, 2017]; afterward the model improved by Spada and Melini [2019] did. The present model includes the key variables that control deformation of the sea floor, and we used the best data available for bathymetry, ice, rheology, and other variables. A map resulting from a run for 20,000 BP was published and long term trends were summarized verbally in *Geographical Review* [Dobson et al., 2020b]. Map results for 30,000 through 21,500 BP and 19,500 through 500 BP are published here for the first time.

We checked our results against the leading alternative model, indeed the only other model in this category, and the two sets of results agree. Both models have been calibrated by their authors using numerous sea-level proxies since the LGM. The same islands appear consistently in multiple runs over thousands of years. Thus, we believe our model is robust and the results are as trustworthy as model results can be.

Using a GIA model, Clark et al. [2014] found an "elaborate archipelago ... that may have served as occupation sites", but they did not speculate on its role in migration. They used a 1000 year time interval and concluded, "in archaeological applications ... predictions of shoreline evolution require a precision better than ~1 kyr" (as we have done with our 500-year interval).

Zimmermann and Prescott [2018] meticulously compiled an accurate and precise map of the eastern Bering Sea floor. In so doing, they found errors in the widely used and highly respected ETOPO1 bathymetry database [Amante and Eakins, 2009]. We relied on that same database, which we still consider to be the best available for the entire world ocean, in our analysis of global choke points at Last Glacial Maximum [Dobson et al., 2020b]. We are concerned about any effect ETOPO1 errors may have had *in certain locations, constrained to the horizontal extent of the errors themselves* [Dobson et al., 2020a]. Bathymetry is crucial, but our model is driven also by density and rheological parameters, a set of "Love numbers", a sea-level equation, and the geometry and temporal evolution of ice sheets.

The errors found by Zimmermann and Prescott were predominantly negative, meaning ETOPO1 showed deeper bottom than Zimmermann and Prescott determined from other trusted sources. Only positive ones can cause false positive islands in our model. Conversely, if we show a transitory island on top of a negative error, our model must be robust enough to overcome the disadvantage associated with that error. Thus, the net effect of the errors they found would be to underestimate, not overestimate, the number and size of transitory islands.

Ice history

Lambeck et al. [2002] and Peltier et al. [2015] show the Gulf of Alaska in the vicinity of our islands and long stretches of the Alaska coast to have been ice-free for extensive periods during the Late Pleistocene ice ages. Keep in mind, however, that they are focused on the mass of ice creating isostatic pressures. Were these same locations ice-free in terms of paddling and landing skin boats? For instance, Lambeck's model does not consider sea-ice since it is irrelevant to computation of Glacial Isostatic Adjustment.

Could our transitory islands have been surrounded by floating "sea" ice? Caissie et al. [2010] conclude, "After the LGM, the Bering Sea experienced a warming driven by increasing high northern latitude insolation. In response, sea ice coverage at Umnak Plateau declined from thick, perennial ice to ice-free conditions in the deep, southeastern Bering Sea". Umnak is 200 km southwest of Unimak Pass and thus a good surrogate for conditions there. Pelto et al. [2018] say "In the Bering Sea, deglaciation began around 18–17 ka". Matul [2017] proposed different limits for winter sea-ice during LGM, some covering all of Beringia. He describes seasonal ice with open conditions in summer. The absence of permanent sea ice in interglacial periods is confirmed by Detlef et al. [2018] in previous epochs (Pleistocene); we believe there is no reason to assume the behavior of sea ice at LGM would be strongly different from previous glacial–interglacial cycles.

30,000-year animation of sea levels in the Bering Strait

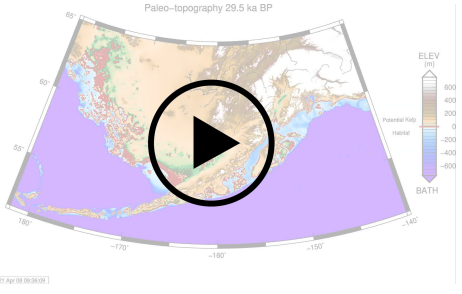

(video available at https://doi.org/10.5802/crgeos.53)

From at least 30,000 BP to 20,500 BP (LGM), islands and coastal lands emerged as the ocean fell. We cannot model sea level any earlier than 30,000 BP due to a lack of reliable ice data. Hence, we cannot say when the archipelago initially formed, but we can say it was intact at 30,000 BP. The animation then shows

a steady retreat of sea level over a broad front reaching maximum land area at 20,500 BP. For analysis, we arbitrarily divided the arc of the Beringian shoreline into three equal sections. The westernmost section started with a few scattered islands which did not increase in number, but coastal lands grew seaward at a rapid pace. The middle section was crowded with islands and contained a shoreward bulge of Beringia. At coarse scale the islands changed little over time, but details of size, shape, and location shifted continuously. Meanwhile Beringia itself grew seaward at a rapid pace. The eastern section had few islands but one did appear early and many small ones later appeared near the advancing shore. Across all three sections, the general pattern remained the same, except that the bulge of the middle section expanded prominently.

The ocean rose from 20,500 BP to 8000 BP. Most islands and coastal lands remained for thousands of years, then gradually submerged to the present shorelines. From 20,500 BP to 19,000 BP rising seas rapidly inundated land especially in the western and eastern sections, and loss of coastal mainland was more conspicuous than loss of islands. From 18,500 BP to 10,500 BP the main shoreline retreated at a steady pace, forming and leaving many small islands in its wake.

According to our model, the Bering Strait reopened at 10,000 BP (Figure 1), a thousand years later than one recent estimate [Jakobsson et al., 2017]. By that time only three islands remained in the western section. The vast majority of all remaining islands were in the middle section where the outline of their distribution spanned most of the area previously covered by the Bering mainland. The eastern section had few islands in the early millennia but many relatively large ones near shore at 10,000 BP.

From 10,000 BP to 8000 BP islands and mainland disappeared at astonishing rates. The middle section lost by far the most land in number and area of islands and coastal mainland. Most islands, except those which remain today, were lost by 8000 BP, but coastal lands continued to inundate substantially through 6500 BP and gradually through 1000 BP.

This constantly changing pattern of island formation and inundation meant that Asian peoples could have settled the western section anytime between 30,000 BP and about 19,000 BP. For thousands of years residents could have seen the westernmost islands from shore and sailed, paddled, or drifted to them with a short voyage of, say, 10 to 20 km. Once in the archipelago, island residents could have continued eastward on a short voyage to nearby islands any time before 15,000 BP when the distribution of islands in the western section first became sparse. Afterward so many western islands submerged that the pathway eastward from Siberia to the middle section became less attractive.

The theater of operations then would have shifted to the middle section. The northernmost islands were visible and accessible from shore with a short sail, paddle, or drift. Residents of the archipelago could have voyaged to neighboring islands in the middle section and onward into the eastern section anytime between 10,000 BP and 7500 BP. This final phase would have been steady attrition as islands were lost first in the middle section and then the eastern section. The phase from 10,000 BP to 8000 BP was mainly a gradual shift from dense to sparse island distribution. Then the rising sea relentlessly forced residents to evacuate eastward toward North America and ultimately to land on its shores. After 7500 BP no islands remained except those present today but coastal lands were still being lost at a steady, relatively slow pace.

Potential bull kelp habitat is a special elevation category shown within the 61-map animation. It is highlighted as a red pattern consisting of all seafloor from −3 to −20 m in depth. We do not have sufficient geologic data to distinguish where kelp will actually grow within the potential area defined solely by depth.

References

Amante, C. and Eakins, B. W. (2009). ETOPO1 1 arc-minute global relief model. In *NOAA Technical Memorandum NESDIS NGDC-24, Boulder, Colorado*.

Caissie, B. E., Brigham-Grette, J., Lawrence, K. T., Herbert, T. D., and Cook, M. S. (2010). Last Glacial Maximum to Holocene sea surface conditions at Umnak Plateau, Bering Sea, as inferred from diatom, alkenone, and stable isotope records. *Paleoceanography*, 25.

Clark, J., Mitrovica, J. X., and Alder, J. (2014). Coastal paleogeography of the California–Oregon–Washington and Bering Sea continental shelves

during the latest Pleistocene and Holocene: implications for the archaeological record. *J. Archaeol. Sci.*, 52, 12–23.

Detlef, H., Belt, S. T., Sosdian, S. M., Smik, I., Lear, C. H., Hall, I. R., Cabedo-Sanz, P., Husum, K., and Kender, S. (2018). Sea ice dynamics across the Mid-Pleistocene transition in the Bering Sea. *Nat. Commun.*, 9, 1–11.

Dobson, J. E. (2014). Aquaterra *Incognita*: Lost land beneath the sea. *Geograph. Rev.*, 104, 123–138.

Dobson, J. E., Spada, G., and Galassi, G. (2020a). An evidence-based reioinder to Zimmermann and Prescott. *Geograph. Rev.*, 110(4), 623–624.

Dobson, J. E., Spada, G., and Galassi, G. (2020b). Global Choke Points May Link Sea Level and Human Settlement at the Last Glacial Maximum. *Geograph. Rev.*, 110, 1–26.

Jakobsson, M., Pearce, C., Cronin, T. M., Backman, J., Anderson, L. G., Barrientos, N., Björk, G., Coxall, H., De Boer, A., and Mayer, L. A. (2017). Post-glacial flooding of the Bering Land Bridge dated to 11 cal ka BP based on new geophysical and sediment records. *Clim. Past*, 13, 991.

Lambeck, K. and Chappell, J. (2001). Sea level change through the Last Glacial Cycle. *Science*, 292, 679–686.

Lambeck, K., Purcell, A., Johnston, P., Nakada, M., and Yokoyama, Y. (2003). Water-load definition in the Glacio-hydro-isostatic Sea-level Equation. *Quater. Sci. Rev.*, 22, 309–318.

Lambeck, K., Yokoyama, Y., and Purcell, T. (2002). Into and out of the Last Glacial Maximum: Sea-level change during Oxygen Isotope Stages 3 and 2. *Quater. Sci. Rev.*, 21, 343–360.

Martinec, Z., Klemann, V., van der Wal, W., Riva, R., Spada, G., Sun, Y., Melini, D., Kachuck, S., Barletta, V., Simon, K., et al. (2018). A benchmark study of numerical implementations of the Sea Level Equation in GIA Modelling. *Geophys. J. Int.*, 215, 389–414.

Matul, A. G. (2017). Probable limits of sea ice extent in the northwestern Subarctic Pacific during the last glacial maximum. *Oceanology*, 57, 700–706.

Peltier, W. R. (1994). Ice Age paleotopography. *Science*, 265, 195–201.

Peltier, W. R., Argus, D. F., and Drummond, R. (2015). Space geodesy constrains Ice Age terminal deglaciation: The Global ICE-6G_C (VM5a) Model. *J. Geophys. Res.: Solid Earth*, 120, 450–487.

Pelto, B. M., Caissie, B. E., Petsch, S. T., and Brigham-Grette, J. (2018). Oceanographic and Climatic Change in the Bering Sea, Last Glacial Maximum to Holocene. *Paleoceanogr. Paleoclimatol.*, 33, 93–111.

Spada, G. and Galassi, G. (2017). Extent and dynamic evolution of the lost land aquaterra since the Last Glacial Maximum. *C. R. Geosci.*, 349, 151–158.

Spada, G. and Melini, D. (2019). SELEN4 (SELEN version 4.0): a Fortran program for solving the gravitationally and topographically self-consistent sea-level equation in glacial isostatic adjustment modeling. *Geosci. Model Dev.*, 12(12), 5055–5075.

Tegmark, M. (1996). An icosahedron-based method for pixelizing the Celestial Sphere. *Astrophys. J.*, 470.

Zimmermann, M. and Prescott, M. M. (2018). Bathymetry and Canyons of the Eastern Bering Sea Slope. *Geosciences*, 8, 184.

Zong, C. (2015). Late Pleistocene sea levels and resulting changes in global land distributions.